

Light-Responsive Elastin-Like Peptide-Based Targeted Nanoparticles for Enhanced Spheroid Penetration

Citation for published version (APA):

Le, D. H. T., Ibrahimova, V., van den Wildenberg, S. A. H., Wu, H., Fonseca, A., Torres, T., Garanger, E., Leenders, W. P. J., Brock, R., Lecommandoux, S., & van Hest, J. C. M. (2023). Light-Responsive Elastin-Like Peptide-Based Targeted Nanoparticles for Enhanced Spheroid Penetration. *Angewandte Chemie - International Edition*, 62(24), Article e202300511. <https://doi.org/10.1002/anie.202300511>

DOI:

[10.1002/anie.202300511](https://doi.org/10.1002/anie.202300511)

Document status and date:

Published: 12/06/2023

Document Version:

Publisher's PDF, also known as Version of Record (includes final page, issue and volume numbers)

Please check the document version of this publication:

- A submitted manuscript is the version of the article upon submission and before peer-review. There can be important differences between the submitted version and the official published version of record. People interested in the research are advised to contact the author for the final version of the publication, or visit the DOI to the publisher's website.
- The final author version and the galley proof are versions of the publication after peer review.
- The final published version features the final layout of the paper including the volume, issue and page numbers.

[Link to publication](#)

General rights

Copyright and moral rights for the publications made accessible in the public portal are retained by the authors and/or other copyright owners and it is a condition of accessing publications that users recognise and abide by the legal requirements associated with these rights.

- Users may download and print one copy of any publication from the public portal for the purpose of private study or research.
- You may not further distribute the material or use it for any profit-making activity or commercial gain
- You may freely distribute the URL identifying the publication in the public portal.

If the publication is distributed under the terms of Article 25fa of the Dutch Copyright Act, indicated by the "Taverne" license above, please follow below link for the End User Agreement:

www.tue.nl/taverne

Take down policy

If you believe that this document breaches copyright please contact us at:

openaccess@tue.nl

providing details and we will investigate your claim.

Nanoparticles

Light-Responsive Elastin-Like Peptide-Based Targeted Nanoparticles for Enhanced Spheroid Penetration

Duc H. T. Le, Vusala Ibrahimova, Sebastian A. H. van den Wildenberg, Hanglong Wu, Alba Fonseca, Tomas Torres, Elisabeth Garanger, William P. J. Leenders, Roland Brock, Sébastien Lecommandoux, and Jan C. M. van Hest*

Abstract: We describe here a near infrared light-responsive elastin-like peptide (ELP)-based targeted nanoparticle (NP) that can rapidly switch its size from 120 to 25 nm upon photo-irradiation. Interestingly, the targeting function, which is crucial for effective cargo delivery, is preserved after transformation. The NPs are assembled from (targeted) diblock ELP micelles encapsulating photosensitizer TT1-monoblock ELP conjugates. Methionine residues in this monoblock are photo-oxidized by singlet oxygen generated from TT1, turning the ELPs hydrophilic and thus trigger NP dissociation. Phenylalanine residues from the diblocks then interact with TT1 via π - π stacking, inducing the re-formation of smaller NPs. Due to their small size and targeting function, the NPs penetrate deeper in spheroids and kill cancer cells more efficiently compared to the larger ones. This work could contribute to the design of “smart” nanomedicines with deeper penetration capacity for effective anticancer therapies.

Introduction

Nanoparticles (NPs) self-assembled from (bio-)macromolecules, while holding great potential for (targeted) nanomedicine, fail most of the time in translational trials.^[1] One of the major hurdles is the limited tissue penetration of NPs due to the presence of complex biological barriers in the tumor microenvironment (TME) such as aberrant vascularization, dense extracellular matrix fibrosis and increased interstitial fluid pressure.^[1] The current state-of-the-art NPs typically have average sizes of 100 nm or larger, which are favorable for longer circulation time and tumor accumulation.^[2] However, this does not lead to improved therapeutic effects due to limited tissue penetration.^[2] A new trend in nanovehicle development is to construct NPs that are responsive to endogenous stimuli such as low pH or enzymes in the TME for changing their size.^[3,4] However, employing external stimuli such as light to induce a size change for improving tissue penetration has been

underexplored.^[4] Moreover, short-term irradiation triggering a rapid response might also benefit cargo release.

NIR light (650–900 nm) is a highly efficient stimulus offering precise spatiotemporal control. It is currently exploited in photodynamic therapy (PDT) as a non-invasive approach for anticancer treatment and is typically combined with chemotherapy or immunotherapy to achieve synergistic effects.^[5] PDT requires delivery of non-toxic photosensitizers (PSs) to the treatment sites where, only upon photo-irradiation, they generate highly toxic reactive oxygen species (ROS), which damage targets via oxidation. Various designs of self-assembling polymers and peptides have been developed for PS delivery and recently also for triggered release, in most cases intracellularly. Wang et al. exploited micellar systems based on selenium-containing block copolymers encapsulating doxorubicin and the PS indocyanine green.^[6] Following cellular uptake, the particles disassembled rapidly upon light irradiation, due to ROS-mediated oxidation of selenium and released co-encapsulated

[*] Dr. D. H. T. Le, S. A. H. van den Wildenberg, Dr. H. Wu, Prof. Dr. J. C. M. van Hest
 Department of Biomedical Engineering, Institute for Complex Molecular Systems (ICMS), Eindhoven University of Technology
 PO Box 513, 5600 MB Eindhoven (The Netherlands)
 E-mail: J.C.M.v.Hest@tue.nl

Dr. D. H. T. Le, Dr. W. P. J. Leenders, Prof. Dr. R. Brock
 Department of Medical BioScience, Radboud Institute for Molecular Life Sciences (RIMLS), Radboud University Medical Center
 Geert Grooteplein 28, 6525 GA Nijmegen (The Netherlands)

Dr. V. Ibrahimova, Dr. E. Garanger, Prof. Dr. S. Lecommandoux
 Université Bordeaux, CNRS, Bordeaux INP, LCPO, UMR 5629
 33600 Pessac (France)

A. Fonseca, Prof. Dr. T. Torres
 Departamento de Química Orgánica and Institute for Advanced Research in Chemical Sciences (IAdChem),
 Universidad Autónoma de Madrid
 28049 Madrid (Spain)

Prof. Dr. R. Brock
 Department of Medical Biochemistry, College of Medicine,
 Arabian Gulf University
 Manama 293 (Kingdom of Bahrain)

© 2023 The Authors. Angewandte Chemie International Edition published by Wiley-VCH GmbH. This is an open access article under the terms of the Creative Commons Attribution Non-Commercial License, which permits use, distribution and reproduction in any medium, provided the original work is properly cited and is not used for commercial purposes.

doxorubicin. In another study, synthetic peptides were co-assembled with the porphyrin Ce6. The system also responded quickly to light irradiation and dissociated into both smaller micellar structures (≈ 85 nm) and fibrils (> 700 nm in length),^[7] enhancing tumor retention of cargos and showing high cell-killing capacity in vitro and in vivo. The sizes after transformation were, however, larger than optimal (< 30 nm) for tissue penetration. Another approach to improve on therapeutic efficacy is the incorporation of a targeting function, as shown for example for PDT treatment.^[8,9] Unfortunately, particle dissociation is often not compatible with targeting, as the latter function is lost when the particles are disassembled. Here we present a novel polypeptide-based NP system that includes (1) rapid light-responsiveness to dissociate into smaller clusters for enhanced tissue penetration and (2) targeted cellular delivery of PSs for highly efficient PDT. The system was designed in a way that the targeting function was preserved after dissociation, thereby overcoming some of the limitations of current stimulus-responsive (targeted) delivery systems.

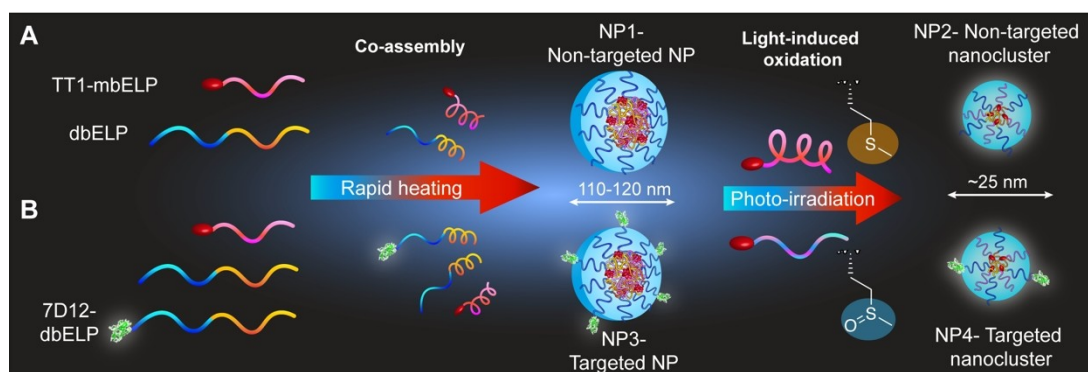
Elastin-like polypeptides (ELPs) are a class of temperature-responsive biopolymers that can be produced in sub-gram scales per liter culture from *E. coli*. They are tailor-made polymers with a high degree of sequence control.^[10] Sequence designs of ELPs are based on the pentapeptide (GXGVP) repeating motif from human elastin protein, where the guest residue X can be any amino acid except for proline. ELPs are routinely referred to as $[A_xB_y-n]$, where A and B indicate the different guest residues, x and y are their corresponding ratios, and n is the total number of pentapeptide repeats. An intrinsic property of ELPs is that upon heating above a specific transition temperature corresponding to their cloud point T_{cp} , the polymers reversibly switch from soluble monomers (hydrophilic state) into insoluble coacervates (hydrophobic state).^[11] Rational design using combinations of $[A_xB_y-x,y,n]$ allows precise control over T_{cp} and/or further endows the polypeptides with additional responsiveness to stimuli like pH or ions.^[12,13] Recently, Ibrahimova et al. constructed a hydrophobic ELP $[M_1V_3-40]$ with methionine (Met, M) and valine (Val, V) guest residues and conjugated it to TT1,^[14] a NIR wavelength (650–660 nm) absorbing phthalocyanine-based PS with superior photo-physical properties.^[15,16] Upon light irradiation, the thioether groups from the Met side chains were photo-oxidized into sulfoxide groups by ROS generated from TT1.^[14] As a result, the photo-oxidized ELP became more hydrophilic leading to a shift to a higher T_{cp} .^[14,17] This light-responsive switch could thus be employed as a smart tool to control the disassembly of NPs. As $[M_1V_3-40]$ by itself formed micron-sized coacervates rather than NPs, we employed the co-assembly approach described by Pille et al. to prepare homogeneous micellar NPs.^[18] The co-assembly approach is a kinetic-driven pathway in which a mixture of an amphiphilic diblock (db) ELP and a monoblock (mb) ELP is rapidly heated above the T_{cp} of the hydrophobic block of dbELP and the T_{cp} of the mbELP. As a result, the mbELP is kinetically entrapped within the hydrophobic core of the micelles formed by the dbELP. Cargos, when conjugated with the

mbELP, are co-encapsulated, allowing efficient loading in a one-step assembly.

In this work, we employed a dbELP with the sequence denoted as $[A_3G_2-60]-[V_4F_1-50]$, which forms micelles above 28 °C (Figures S1 and S2), and the PS-mbELP conjugate TT1- $[M_1V_3-40]$ ^[14] for preparing co-assembled NPs. The guest residue phenylalanine (Phe, F) was introduced in the hydrophobic block $[V_4F_1-50]$ for enhanced stability of the micelle's hydrophobic core via π - π stacking and to provide interaction with TT1. For targeting purposes, the anti-epidermal growth factor receptor (EGFR) nanobody 7D12^[19] was selected as the targeting module and genetically fused to the N-terminus of the hydrophilic block $[A_3G_2-60]$ of the dbELP (7D12-dbELP). This nanobody was previously employed in targeted ELP NP systems developed by our group for PDT applications.^[8] The targeted NP has high affinity and is highly selective towards EGFR-positive cells, resulting in highly efficient PDT treatment.^[8] After co-assembly, 7D12 moieties will be exposed and accessible for EGFR binding followed by NP internalization.^[8,18] Upon light irradiation, photo-oxidation makes the encapsulated TT1- $[M_1V_3-40]$ hydrophilic, triggering instability in the hydrophobic core and disassembly. The designed interaction between Phe residues and TT1 should however yield the formation of smaller clusters in which the nanobody and PS function are kept after transformation. The schematic of particle formation and the disassembly pathway upon light irradiation is shown in Scheme 1.

Results and Discussion

ELPs were synthesized in *E. coli* and purified using the established Inverse Transition Cycling method (Supporting Information). The co-assembled NPs were prepared by adding pre-heated PBS into the mixture of dbELP, TT1-mbELP, and with or without 7D12-dbELP to induce rapid micelle formation and encapsulation of the conjugate. NP preparation is detailed in Supporting Information. First, dynamic light scattering (DLS) was used to determine the size and dispersity of the co-assembled NPs. As shown in Figures 1A and S3A, the co-assembled NPs had a hydrodynamic diameter of 117 ± 27 nm, with a polydispersity index (PDI) of 0.14, indicating a relatively monodispersed population. The targeted NPs also had a similar diameter of 124 ± 46 nm (PDI 0.19) (Figures 1B and S3B). Co-assembled NPs were significantly larger than NPs assembled from the dbELP alone (45 ± 15 nm, Figure S2). The TT1-mbELP conjugate itself only formed ill-defined micron-sized coacervates at 37 °C.^[14] The combined data indicate that the TT1-mbELP conjugates were encapsulated within the dbELP during co-assembly. To study the light-responsiveness, a 660 nm laser light source (0.12 W cm^{-2}) was used to irradiate the particle suspension for 5 min, followed by DLS at 37 °C. Photo-irradiation led to a shift to smaller sizes for both non-targeted and targeted micelles, 25 ± 9 nm (PDI 0.12) and 25 ± 7 nm (PDI 0.21) respectively (Figures 1A, 1B, and S3). Photo-oxidation of encapsulated TT1-mbELP was further analyzed with denaturing gel electrophoresis SDS-PAGE in



Scheme 1. Schematic of the formation of co-assembled NPs without (A) and with (B) the targeting ligand (EGFR-targeting nanobody 7D12). Upon light irradiation, the NPs rapidly disassemble because of photo-oxidation of the Met-containing monoblock ELP carrying the photosensitizer (TT1-mbELP), which is encapsulated within the NPs formed by the diblock (db) ELPs. The hydrophobicity-to-hydrophilicity shift induces disassembly, while π - π stacking of the TT1 photosensitizer with the Phe residues of the dbELP, including the 7D12 containing dbELP (7D12-dbELP), results in reorganization in smaller (targeted) nanoclusters.

which a molecular weight shift was observed of the fluorescent TT1-[M₁V₃-40] (Figure 1C). Similarly, a shift in elution of TT1-[M₁V₃-40] upon light treatment was detected (Figure 1D). Deconvoluted masses of these peaks indicated that five to seven thioethers of the in total eleven Met residues were oxidized (Figure S4 and Table S2). The photo-oxidized TT1-mbELP, with a higher T_{cp} , became more hydrophilic,^[14] which triggered instability and disassembly of the co-assembled NPs. Hereafter, the non-targeted and targeted NPs without light treatment are named NP1 and 3, respectively. After light irradiation, NP1 and 3 were converted into non-targeted NP2 and targeted NP4, respectively.

The morphologies of these NPs were further confirmed by cryogenic transmission electron microscopy (cryo-TEM). As shown in Figure 1E, NP1 had a spherical morphology with the size ranging from 80–110 nm. Due to temperature fluctuations and the presence of ambient light during sample preparation for imaging, the observed particle sizes might be affected and appeared to be more polydisperse. Multiple black dots were also observed within the NP; this higher electron density could be attributed to the stacking of multiple TT1 bearing zinc atoms. Given that the hydrophobic block contains multiple Phe guest residues, there might be also interaction with TT1 via π - π stacking. Upon light irradiation, significantly smaller-sized protein clusters (NP2) were observed, with a size of approximately 10 nm (Figures 1E and S5). Because cryo-TEM only reflected the condensed hydrophobic core, this might explain the smaller size compared to DLS measurements. The morphologies looked homogeneous even though they consisted out of multiple ELP species. Moreover, they were also different from micelles assembled from dbELP alone which have a larger hydrophobic core as seen in our previous work.^[13] These findings strongly suggest that the clusters were composed of both dbELP and photo-oxidized TT1-mbELP. The hydrophilic region was now extended to both the [A₃G₂-60] domain from the dbELP and the oxidized [M₁V₃-40] domain, both of which played a role in colloid

stabilization (Scheme 1). The two ELPs were kept together through π - π stacking between the Phe residues and TT1. Overall, DLS and cryo-TEM results together confirmed the formation of NPs using the co-assembly method and their re-organization upon photo-irradiation. The targeted NP3 and the targeted nanoclusters (NP4) showed similar characteristics, and no differences were observed with cryo-TEM (Figures 1E and S5) and DLS measurements (Figures 1A and 1B) compared to NP1 and 2, respectively. Furthermore, UV/Vis spectroscopy also did not show differences between ELP NP1–4; all had a broad absorbance between 600–700 nm with the peak at 630 nm, indicative of the presence of TT1 (Figure S6). The nanoclusters were expected to also contain the nanobody, as 7D12 was conjugated to the same Phe residues-containing dbELP. This would endow the nanoclusters with a targeting function. To unambiguously demonstrate its presence, cell uptake studies were performed.

We thus investigated the interaction of NP1–4 with the EGFR-expressing human carcinoma cell line A431^[20] to study their targeting functions. The uptake pathways of the NPs were monitored spectroscopically via TT1 fluorescence (Ex/Em 630/660 nm), which was conjugated to the mbELP, and via Cy3 fluorescence (Ex/Em 550/580 nm) attached to the N-terminus of the dbELP. After incubation for 1.5–3 hours, cells were washed and imaged live using confocal microscopy. Uptake of the targeted NP3 was already observed within 1.5 hours while there was no signal observed for NP1 up to 3 hours (Figures S7 and 2A). The punctate intracellular signals suggest that NP3 was endocytosed. The Pearson's coefficients of TT1 and Cy3 from NP3 after 1.5 and 3 hours were 0.80 and 0.78, respectively, indicating the presence of intact NPs. We then sought to explore the behavior of the nanoclusters toward cell uptake, and especially to learn whether the targeting function was preserved. Similar to NP1, NP2 did not show uptake after 1.5 and 3.0 hours (Figures S7 and 2A). In the case of NP4, the signals of Cy3 and TT1 were detected in both time points (Figures S7 and 2A). Because only 10 % dbELP was

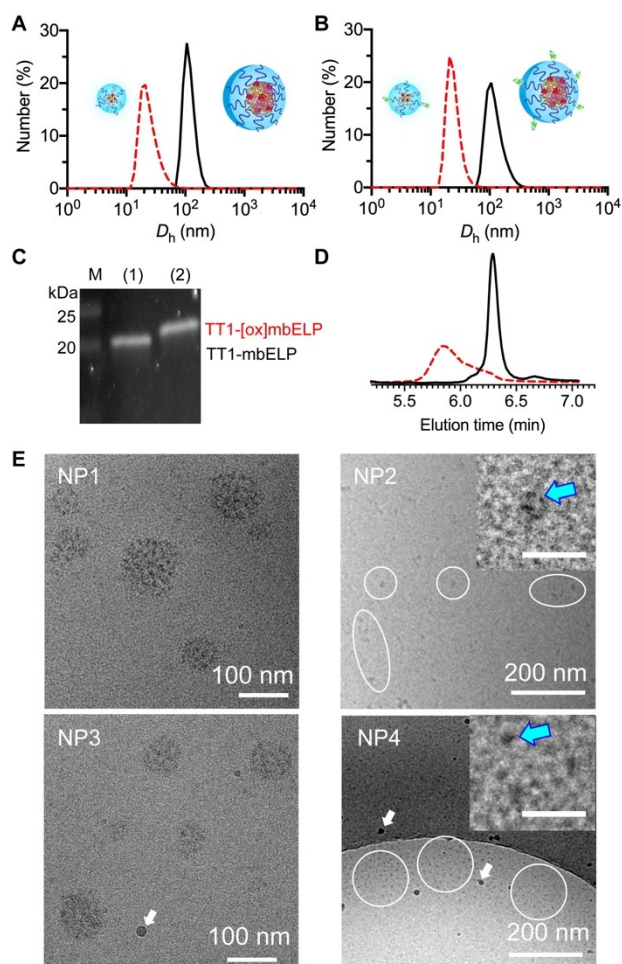


Figure 1. Characterization of ELP NPs. DLS profiles of (A) non-targeted NPs before (NP1-black line) and after light irradiation (NP2-red dotted line), and (B) targeted NPs before (NP3) and after light irradiation (NP4). (C) SDS-PAGE of TT1-mbELP encapsulated within the co-assembled NP before (1) and after (2) light irradiation (TT1-[ox]mbELP). M: marker. Protein bands were visualized via TT1 fluorescence under UV light. Uncropped image is shown in Figure S15. (D) Elution profiles of TT1-mbELP before (black) and after (dashed red) light irradiation using the Polaris C8 column. (E) Cryo-TEM imaging of NP1–4. The nanoclusters are shown in white circles. Zoom-in images of NP2 and 4 are further shown in inset (scale bar 25 nm), with the blue arrows pointing to the clusters. The black spots with blurred edges, indicated with white arrows, correspond to ice crystals.

labeled with Cy3, some nanoclusters which were formed with non-labeled dbELP were visualized via only the TT1 signal, resulting in differences in Cy3 and TT1 intensities. The Pearson's coefficients of TT1 and Cy3 from NP4 were 0.35 and 0.66 after 1.5 and 3 hours, respectively, both of which were lower than the ones from NP3. While it is more complicated to compare the coefficients at the later stage (3 hours) due to cellular processes in endosomes, there was a significant difference in the coefficients between NP3 and NP4 at 1.5 hours. This evidence of different Cy3 and TT1 distribution again confirmed disassembly. After 3 hours, the mean fluorescence intensity (FI) from Cy3 and TT1 originating from NP3 was 1.8-fold and 1.5-fold higher,

respectively than for NP4 (Figure S8). NP1 and NP2 showed negligible mean FI (Figure S8). Overall data suggested that signals in NP4 was the consequence of targeted delivery and that 7D12-dbELP and TT1-mbELP co-clustered after light irradiation. In line with the cell uptake study, intracellular ROS production, upon photo-irradiation for 15 min, was also observed for NP3 and 4 (Figures 2B and S10) but not for NP1 and NP2 in A431 cells. We also tested NP1–4 using another EGFR-positive MDA-MB-468 cell line,^[21] in which a similar uptake phenomenon was observed for NP3 and NP4 (Figure S9).

To see whether the smaller sized nanoclusters would show enhanced tissue penetration, we incubated the above platforms for 3 hours with 250–300 μm spheroids grown from A431 cells as a tumor tissue mimicking in vitro model. Spheroids were then washed with PBS and fixed using paraformaldehyde before embedding them in collagen gels for imaging. To visualize the core of the spheroids, which is limited by the laser penetration depth, a clearance step using a fructose solution was performed.^[22] There were limited signals from Cy3 and TT1 from NP1 (Figure 3A), indicating that only few particles had accumulated in the spheroids due

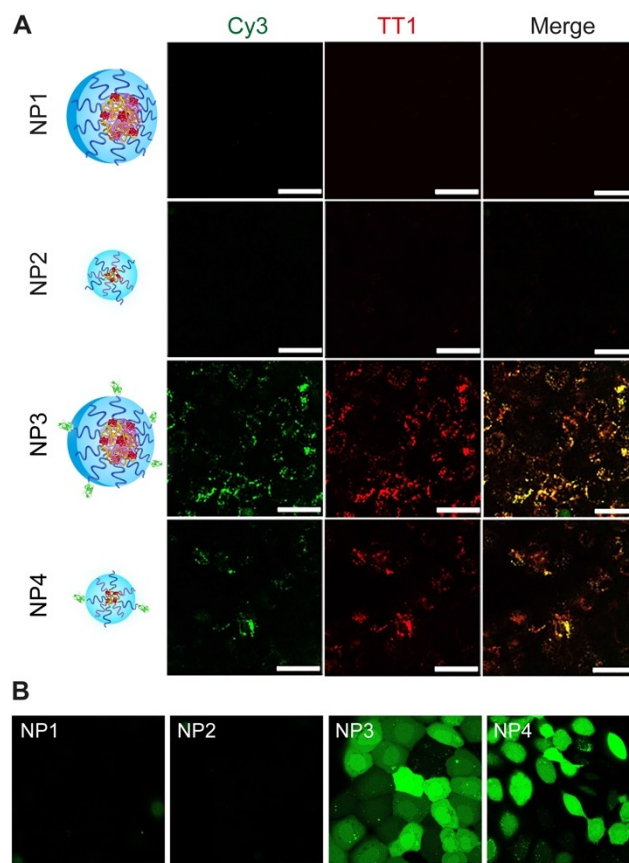


Figure 2. (A) Cell uptake of NP1–4 in A431 cells after 3 hours. DbELP was visualized via Cy3 channel and TT1-mbELP was visualized via TT1 channel. (B) Detection of intracellular reactive oxygen species (ROS) via the DCFH-DA fluorescence probe in A431 cells. ROS was detected after 15 min light irradiation of A431 cells treated with NP3 and NP4 for 3 hours but not seen in ones conducted with NP1 or NP2. Scale bar 50 μm .

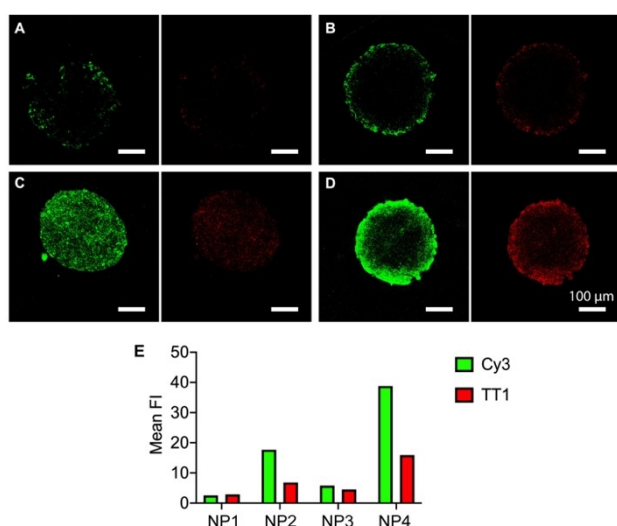


Figure 3. Penetration profiles of ELP NPs into A431 spheroids after 3 hour incubation. (A) NP1, (B) NP3, (C) NP2 and (D) NP4. Cy3 (dbELP) and TT1 (mbELP) channels are depicted in green and red, respectively. (E) Mean fluorescence intensity (FI) of Cy3 and TT1 from NP1–4 in the equatorial planes of the spheroids.

to the lack of a targeting function and the size limitation (>100 nm). By comparison, NP3 showed higher TT1 and Cy3 intensities (Figure 3B), mostly found at the periphery of the spheroid because of size limitations. In contrast, nanoclusters showed greater diffusion into spheroids due to their relatively small sizes. For NP2, signals from Cy3 and TT1 were distributed homogeneously throughout the spheroids (Figure 3C). For NP4, fluorescence showed a gradient from the edge towards the center which can be explained by a binding-site barrier (Figure 3D).^[23] It should be noted that the detected signals do not reflect whether NPs were located intra- or extracellularly. Cy3 and TT1 fluorescence intensity distributions along the diameters of spheroids in Figure 3A are shown in Figures S11 and S12. The data indicated that indeed the nanoclusters (NP2 and NP4) had not only enhanced penetration but also higher accumulation, reflected by the higher intensities of both Cy3 and TT1. Mean FI at the equatorial planes of spheroids indicated that NP4 had ≈ 2 -fold higher signals of Cy3 and TT1 compared to NP2, demonstrating the activity of the targeting function (Figure 3E). NP4 also outperformed NP1 and NP3 with ≈ 9.5 -fold higher fluorescence for Cy3 and 4.5-fold higher fluorescence for TT1, respectively (Figure 3E). Overall, these results confirm that small nanoclusters have enhanced penetration compared to intact NPs. While we have utilized 10% of the total ELPs for the targeted ELP, adjusting the percentage of 7D12-dbELP could be further employed in rationally tuning between efficacy for tissue penetration and tissue targeting.

After confirming cellular uptake and tissue penetration, in vitro PDT treatments were conducted in 2D cell layers and 3D spheroids with the expectation that the targeted platforms would outperform non-targeted ones due to the effective delivery of the PS. Before PDT treatment, a dark

toxicity assay was performed to confirm that these ELP nanoplatforms did not have cell-killing effects without light irradiation (Figure S13). Furthermore, irradiation using PS-loaded NPs did not result in a temperature increase (Figure S14); therefore, artifacts from thermal effects can be excluded. We first explored PDT efficiency for cells treated with NP1 and NP3. The TT1-mbELP, which forms microcavates, was also included as a control. After 1.5 hour incubation, A431 cells were treated for 15 min using a 660 nm laser light source (0.12 W cm^{-2}). As shown in Figure 4A, neither the TT1-mbELP conjugate alone nor NP1 showed phototoxicity at $1.0 \mu\text{M}$ of the PS. By comparison, NP3 loaded with $1.0 \mu\text{M}$ TT1 were highly efficacious, with >96% cell killing after illumination and 84% cell killing at $0.25 \mu\text{M}$ TT1. At $0.10 \mu\text{M}$ TT1 still 30.5% cell-killing was observed (Figure 4A). Noteworthy, the effective doses of TT1 in this study were in a sub-micromolar range even though cells were treated only for a relatively short time (1.5 hours) compared to other reported systems,^[24] demonstrating the benefit of active targeting by 7D12. Subsequently, the activities of NP3 and NP4 were compared (Figure 4B). In this 2D tissue culture, there was no significant difference between efficacies of the two platforms

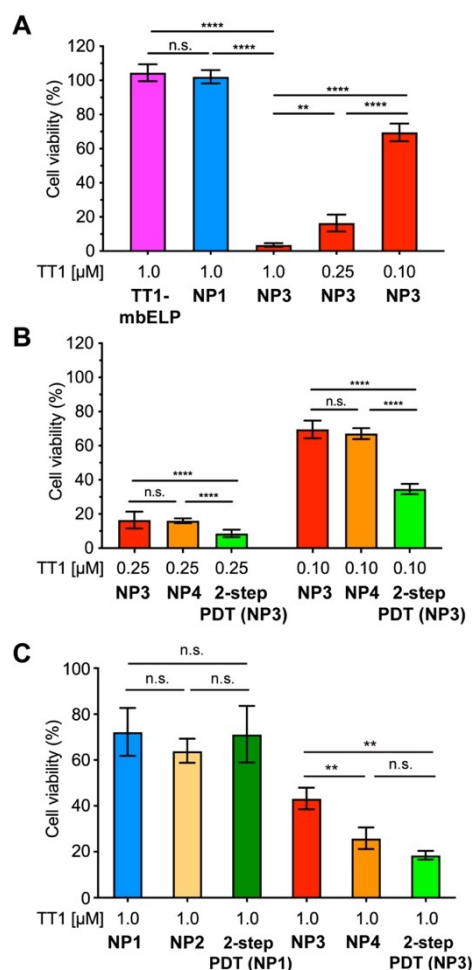


Figure 4. In vitro PDT treatment efficacies studied by cytotoxicity assays in a 2D cell culture (A, B) and in a 3D spheroid (C) model.

at 0.25 μM and 0.10 μM (Figure 4B). In addition, a two-step PDT was also carried out, in which NP3 were first treated by light for 5 min after 30 min incubation to convert them into nanoclusters (NP4). After another 1 hour incubation, a second PDT treatment was carried out for 10 min to induce cell-killing. As shown in Figure 4B, the two-step PDT showed 2-fold enhanced efficiencies (8.6% and 34.7% cell viability) in cell killing at 0.25 and 0.10 μM TT1, respectively. This suggested the 2-step PDT was more efficient as the IC_{50} was shifted to a lower dose range. We hypothesize that targeted NPs (NP3) rapidly bound and were taken up within the first 30 min incubation, allowing high accumulation in A431 cells. The first PDT disassembled NP3 into nanoclusters. The second PDT then led to a higher efficacy because of the increased amount of intracellular NP4. Furthermore, the intracellular disassembly could also lead to a better utilization of TT1 and/or oxygen diffusion, due to diminished stacking or encapsulation in the hydrophobic core as in NP3.^[25,26]

Finally, the efficacies of NP1–4 were tested using A431 spheroids, given that the targeted nanoclusters (NP4) penetrated deeper into the spheroids. Spheroids were incubated with NPs for 24 hours and then irradiated with a 660 nm laser light (0.12 Wcm^{-2}) for 15 min. As shown in Figure 4C, there was no significant difference between NP1 and NP2. Both killed approximately $\approx 27\%$ of cells from the spheroids. NP3 performed better with 57% cells killed, which can be attributed to the targeting function. NP4 outperformed the other formulations with more than 74% cell death, which is consistent with the observed higher tissue penetration (Figure 3) and high efficacies in the 2D experiment (Figure 4B). The two-step PDTs using NP1 and NP3 were also carried out to first deliver intact NPs to tumor tissues and then to disassemble them to form nanoclusters for enhanced tissue penetration and PDT. The first 5 min PDT was performed 3 hours post-incubation to convert NP1 and NP3 into NP2 and NP4, respectively. After another 21 hour incubation, spheroids were treated with 10 min irradiation. The two-step process performed with NP1 showed comparable treatment efficacies as their non-targeted counterparts (NP1 and NP2) (Figure 4C), indicating that no improvement in efficacy was achieved, despite enhanced penetration, likely because of the inefficient intracellular PS delivery. In contrast, spheroids that were incubated initially with NP3 which were then converted into NP4 showed lower viability than the other samples (Figure 4C) with 81.5% cells killed, illustrating the targeted photo-toxicity after disassembly. Importantly, cell killing was as efficient as observed for spheroids directly incubated with NP4.

For future in vivo application, the NPs could be first administered intravenously using the 120 nm targeted NPs (NP3) for longer circulation time and tumor accumulation.^[2] In situ light-irradiation would induce transformation into small NP4 to further facilitate tumor penetration as well as targeted delivery for more efficient treatments. A potential hurdle could be that NP3 is affected from shear stress during circulation leading to phase separation of TT1-mbELP and dbELP before reaching the tumor. Given that ELPs can be

modularly engineered, the stability however can be fine-tuned by controlling for example the number of Phe residues to enhance hydrophobic interactions.

Conclusion

In summary, this work describes a novel design of size-switchable polymeric NPs that rapidly respond to a NIR-light stimulus (5 min) by partial disassembly and re-organizing, while retaining their targeting function and PDT activity. We demonstrate enhanced tissue penetration and highly effective PDT treatment in 2D and 3D in vitro models. The system is based on the co-assembly of various thermo-responsive ELP modules into homogeneous co-assembled NPs by rapid heating.^[18] Generally, ELP NPs are known for their temperature responsiveness. However, for obvious reasons, disassembly of NPs by lowering the temperature cannot easily be applied in vivo. Here we demonstrate that specific disassembly can also be achieved by increasing the T_{cp} in situ by light-induced oxidation of Met-bearing ELPs, giving unique spatiotemporal control. After disassembly, ELP modules, i.e., dbELP and oxidized TT1-mbELP and 7D12-dbELP, likely interact via π - π stacking to form relatively homogeneous small nanoclusters (≈ 24 nm). Therefore, the newly formed nanostructures still have the targeting function, allowing efficient PS delivery and PDT treatment. Such light-responsive targeted systems have not been reported yet to the best of our knowledge. The systems could also be expanded to co-deliver additional cargos via additional conjugation to TT1-mb, such as chemotherapeutics or immunomodulatory factors for multimodal therapies. We believe that this work will contribute significantly to the design of stimulus-responsive NPs that could be potentially used for tackling some of the hurdles in anticancer treatment.

Acknowledgements

This work was supported by EuroNanoMed3 TEMPEAT and SIRIC Brio Commucan projects. We also thank financial support to MINECO (PID2020-116490GB-I00, Porphyrinoids) and PCIN-2017-042, TEMPEAT), the Comunidad de Madrid (MAD2D-CM) and MICINN through project “Materiales disruptivos bidimensionales (2D)” within the Planes Complementarios (Materiales avanzados). The Nouvelle Aquitaine Region and the FRM are also thanked for financial support. IMDEA Nanociencia acknowledges support from the “Severo Ochoa” Programme for Centres of Excellence in R&D (MINECO, Grant SEV-2016-0686).

Conflict of Interest

The authors declare no conflict of interest.

Data Availability Statement

The data that support the findings of this study are available from the corresponding author upon reasonable request.

Keywords: Elastin-Like Peptides · Nanomedicine · Photodynamic Therapy · Self-Assembly · Stimuli-Responsive

-
- [1] M. Izci, C. Maksoudian, B. B. Manshian, S. J. Soenen, *Chem. Rev.* **2021**, *121*, 1746–1803.
- [2] J. Wang, W. Mao, L. L. Lock, J. Tang, M. Sui, W. Sun, H. Cui, D. Xu, Y. Shen, *ACS Nano* **2015**, *9*, 7195–7206.
- [3] A. Banstola, K. Poudel, J. O. Kim, J. H. Jeong, S. Yook, *J. Controlled Release* **2021**, *337*, 505–520.
- [4] Y. R. Zhang, R. Lin, H. J. Li, W. ling He, J. Z. Du, J. Wang, *Wiley Interdiscip. Rev. Nanomed. Nanobiotechnol.* **2019**, *11*, e1519.
- [5] K. Deng, C. Li, S. Huang, B. Xing, D. Jin, Q. Zeng, Z. Hou, J. Lin, *Small* **2017**, *13*, 1702299.
- [6] Y. Wang, Y. Deng, H. Luo, A. Zhu, H. Ke, H. Yang, H. Chen, *ACS Nano* **2017**, *11*, 12134–12144.
- [7] Y. Qin, F. Tong, W. Zhang, Y. Zhou, S. He, R. Xie, T. Lei, Y. Wang, S. Peng, Z. Li, J. Leong, H. Gao, L. Lu, *Adv. Funct. Mater.* **2021**, *31*, 2104645.
- [8] J. Pille, S. A. M. van Lith, J. C. M. van Hest, W. P. J. Leenders, *Biomacromolecules* **2017**, *18*, 1302–1310.
- [9] S. A. M. van Lith, D. van den Brand, R. Wallbrecher, L. Wübbeke, S. M. J. van Duijnoven, P. I. Mäkinen, J. S. Hoogstad-van Evert, L. Massuger, S. Ylä-Herttuala, R. Brock, W. P. J. Leenders, *Eur. J. Pharm. Biopharm.* **2018**, *124*, 63–72.
- [10] D. H. T. Le, A. Sugawara-Narutaki, *Mol. Syst. Des. Eng.* **2019**, *4*, 545–565.
- [11] N. K. Li, F. G. Quiroz, C. K. Hall, A. Chilkoti, Y. G. Yingling, *Biomacromolecules* **2014**, *15*, 3522–3530.
- [12] J. R. McDaniel, D. C. Radford, A. Chilkoti, *Biomacromolecules* **2013**, *14*, 2866.
- [13] M. Abdelghani, J. Shao, D. H. T. Le, H. Wu, J. C. M. van Hest, *Macromol. Biosci.* **2021**, *21*, 2100081.
- [14] V. Ibrahimova, J. A. González-Delgado, M. Levêque, T. Torres, E. Garanger, S. Lecommandoux, *Bioconjugate Chem.* **2021**, *32*, 1719–1728.
- [15] M. García-Iglesias, J. J. Cid, J. H. Yum, A. Forneli, P. Vázquez, M. K. Nazeeruddin, E. Palomares, M. Grätzel, T. Torres, *Energy Environ. Sci.* **2011**, *4*, 189–194.
- [16] G. Martínez-Edo, E. Y. Xue, S. Y. Y. Ha, I. Pontón, J. A. González-Delgado, S. Borrós, T. Torres, D. K. P. Ng, D. Sánchez-García, *Chem. Eur. J.* **2021**, *27*, 14610–14618.
- [17] R. Petitdemange, E. Garanger, L. Bataille, W. Dieryck, K. Bathany, B. Garbay, T. J. Deming, S. Lecommandoux, *Biomacromolecules* **2017**, *18*, 544–550.
- [18] J. Pille, A. Aloï, D. H. T. Le, I. Vialshin, N. van de Laar, K. Kevenaar, M. Merckx, I. K. Voets, J. C. M. van Hest, *Small* **2021**, *17*, 2007234.
- [19] H. Hong, Z. Zhou, K. Zhou, S. Liu, Z. Guo, Z. Wu, *Chem. Sci.* **2019**, *10*, 9331–9338.
- [20] F. Zhang, S. Wang, L. Yin, Y. Yang, Y. Guan, W. Wang, H. Xu, N. Tao, *Anal. Chem.* **2015**, *87*, 9960–9965.
- [21] A. El Guerrab, M. Bamdad, F. Kwiatkowski, Y. Bignon, F. Penault-Llorca, C. Aubel, *Oncotarget* **2016**, *7*, 73618–73637.
- [22] L. M. P. E. van Oppen, J. Pille, C. Stuu, M. van Stevendaal, L. N. van der Vorm, J. A. M. Smeitink, W. J. H. Koopman, P. H. G. M. Willems, J. C. M. van Hest, R. Brock, *Eur. J. Pharm. Biopharm.* **2019**, *137*, 175–184.
- [23] K. Fujimori, D. G. Covell, J. E. Fletcher, J. N. Weinstein, *J. Nucl. Med.* **1990**, *31*, 1191–1198.
- [24] M. Czarnecka-Czapczyńska, D. Aebisher, P. Oleś, B. Sosna, M. Krupka-Olek, K. Dynarowicz, W. Latos, G. Cieślar, A. Kawczyk-Krupka, *Biomed. Pharmacother.* **2021**, *144*, 112342.
- [25] X. Li, M. Ke, M. Zhang, Q. Tang, B. Zheng, J. Huang, *Chem. Commun.* **2015**, *51*, 4704–4707.
- [26] B. Ghazal, A. Husain, A. Ganesan, M. Durmuş, X. Zhang, S. Makhseed, *Dyes Pigm.* **2019**, *164*, 296–304.

Manuscript received: January 11, 2023

Accepted manuscript online: April 21, 2023

Version of record online: May 8, 2023